Structures of Thiolate- and Carboxylate-Ligated Ferric H93G Myoglobin: Models for Cytochrome P450 and for Oxyanion-Bound Heme Proteins † , ‡

5 AUTHORS, INCLUDING:

Lukasz Lebioda

University of South Carolina

138 PUBLICATIONS **2,975** CITATIONS

The Structures of Thiolate- and Carboxylate-Ligated Ferric H93G Myoglobin:

Models for Cytochrome P450 and for Oxyanion-Bound Heme Proteins†

Jie Qin[‡,§], **Roshan Perera**[‡,§], **Leslie L. Lovelace**[§], **John H. Dawson**[*,§,||], and **Lukasz Lebioda**[*,§]
Department of Chemistry and Biochemistry and the School of Medicine, University of South Carolina, Columbia, SC 29208

Abstract

Crystal structures of the ferric H93G myoglobin (Mb) cavity mutant containing either an anionic proximal thiolate sulfur-donor or carboxylate oxygen-donor ligand are reported at 1.7 and 1.4 Å resolution, respectively. The crystal structure and magnetic circular dichroism spectra of the H93G Mb β-mercaptoethanol (BME) thiolate adduct reveal a high-spin, five-coordinate complex. Furthermore, the bound BME appears to have an intramolecular hydrogen bond involving the alcohol proton and the ligated thiolate sulfur, mimicking one of the three proximal N-H···S hydrogen bonds in cytochrome P450. The Fe is displaced from the porphyrin plane by 0.5 Å and forms a 2.41 Å Fe-S bond. The Fe^{3+}-S-C angle is 111 °, indicative of a covalent Fe-S bond with sp^3 hybridized sulfur. Therefore, the H93G Mb·BME complex provides an excellent protein-derived structural model for high-spin ferric P450. In particular, the Fe-S bond in high-spin ferric P450-CAM has essentially the same geometry despite the constraints imposed by covalent linkage of the cysteine to the protein backbone. This suggests that evolution led to the geometric optimization of the proximal Fe-S (cysteinate) bond in P450. The crystal structure and spectral properties of the H93G Mb acetate adduct reveal a high-spin, six-coordinate complex with proximal acetate and distal water axial ligands. The distal His-64 forms a hydrogen bond with the bound water. The Fe-acetate bonding geometry is inconsistent with an electron pair along the Fe-O bond as the Fe-O-C angle is 152° and the Fe is far from the plane of the acetate. Thus, the Fe-O bonding is ionic. The H93G Mb cavity mutant has already been shown to be a versatile model system for the study of ligand binding to heme proteins; this investigation affords the first structural evidence that non-imidazole exogenous ligands bind in the proximal ligation site.

The proximal ligand plays a crucial role in the activation of oxygen and peroxide by heme enzymes (1-5). Although the application of site-directed mutagenesis for the preparation of proximal ligand mutants has yielded important information about their roles in catalysis, the technique is limited by the minimal number of naturally occurring amino acid ligands available in the genetic code. To overcome this shortcoming, Barrick prepared a proximal H93G cavity mutant of sperm whale myoglobin (Mb)[1] by replacing His-93 with a much smaller Gly (6).

‡Contributed equally to this work.
§Department of Chemistry and Biochemistry
||School of Medicine
*Correspondence to Lukasz Lebioda, Phone (803) 777-2140, E-mail: lebioda@mail.chem.sc.edu, John H. Dawson, Phone (803) 777-7234, dawson@mail.chem.sc.edu, Department of Chemistry & Biochemistry, University of South Carolina, Columbia, SC 29208

This creates a proximal pocket that accommodates foreign unnatural ligands, and the H93G Mb cavity mutant has been extensively employed for the preparation of heme protein model complexes (1,7-16) The use of the H93G Mb cavity mutant as a natural protein-derived structural and functional model circumvents the limitations of site-directed mutagenesis. This paper presents the first crystallographic study of the H93G ferric Mb cavity mutant containing non-imidazole proximal ligands, specifically thiolate sulfur and carboxylate oxygen, as structural models for cysteinate- and oxyanion-ligated heme enzymes.

Cysteine serves as a proximal axial ligand in a number of heme enzymes, most notably the dioxygen and peroxide activating enzymes cytochrome P450 (P450), *C. fumago* chloroperoxidase and nitric oxide synthase (2). The cysteine must be deprotonated to cysteinate throughout the reaction cycle for catalytic activity. Dawson has proposed that the cysteinate "push" is important for the mechanism of mono-oxygenase activity in P450 (2,3,17). Various factors that stabilize thiolate ligation have been discussed and investigated (4,10). In particular, there are three amide N-H⋯S(proximal) hydrogen bonds in P450-CAM from residues Leu-358, Gly-359 and Gln-360 that play a key role in the catalytic cycle by helping to retain cysteinate coordination when the iron goes sequentially through the ferric, ferrous and ferryl oxidation states. Morishima and coworkers have used site-directed mutagenesis to remove one of these conserved amide hydrogen bonds in the L358P mutant (18). This led to an increase in the thiolate "push" effect that was proposed to facilitate the protonation of the outer oxygen atom in the hydroperoxo intermediate of P450-CAM. There is no successful natural model system to mimic these highly conserved amide hydrogen bonds although attempts have been made to incorporate hydrogen bonding into synthetic porphyrin models. Nakamura, for example, has prepared ferric porphyrin thiophenolate complexes containing one or two *ortho* substituted amide N-H groups to hydrogen-bond to the coordinated thiolate sulfur (19). The proximal His to Cys mutant of Mb (20,21), H93C Mb, is unable to form a thiolate H-bond with the adjacent amino acid residue, Ser-92, because its hydroxyl group is too far from the Cys-93 S atom.

---

[1]Abbreviations:

H93G myoglobin
     His93Gly variant of sperm whale myoglobin

Mb
     myoglobin

P450
     cytochrome P450

BME
     β-mercaptoethanol

MCD
     magnetic circular dichroism

EA
     electronic absorption

FoFc map
     sigmaa weighted Fourier synthesis with (F_O-F_C) coefficients

2FoFc map
     sigmaa weighted Fourier synthesis with ($2F_O$-F_C) coefficients

PDB
     protein data bank

FePSNP
     the *para*-nitrothiophenol thiolate complex of ferric protoporphyrin IX

A second set of interesting heme proteins has an anionic proximal O-donor ligand, typically tyrosinate, in the ferric state. Some examples are heme containing catalases, the naturally occurring hemoglobin M mutants, and coral allene oxide synthase, all of which contain tyrosinate proximal ligation (22-27). The most notable feature of these proximal oxyanion-ligated proteins is a much lower redox potential compared to neutral His-ligated hemes, sufficiently low so as to make it difficult to naturally reduce the ferric iron to the ferrous state. This is a useful property for enzymes like catalase and allene oxide synthase that need to remain in the ferric state during catalysis, but presents a severe problem for humans with hemoglobin M.

The factors controlling whether an oxyanion-ligated ferric heme center is five-coordinate or six-coordinate with a trans water ligand are not well understood (11). For example, in H93Y Mb, resonance Raman and magnetic circular dichroism (MCD) spectroscopy have shown that it is mostly a five-coordinate species (28,29). Spectroscopic analysis of H25A heme oxygenase at neutral pH reveals a five-coordinate complex with carboxylate ligation to the heme iron (12). Recent MCD characterization of the C436S P450-2B4 mutant revealed a mostly six-coordinate serinate/water-ligated ferric heme center, but the complex is not homogeneous as some portion is five-coordinate (30). Therefore, it is important to examine the contributing factors that influence distal water ligation to oxyanion-ligated (i.e., serinate, tyrosinate or carboxylate) heme iron centers in proteins.

Even though H93G Mb has been used extensively as a probe for modeling heme proteins with O^- and S^- donor proximal ligands (13), there has not been any crystallographic study to show that such ligands bind in the proximal cavity. In the present investigation, we have successfully crystallized the β-mercaptoethanol (BME) and acetate adducts of ferric H93G Mb, and report the structural features observed for these two different proximal donor ligands. The BME thiolate-bound ferric H93G forms a five-coordinate high-spin adduct, while acetate carboxylate-bound ferric H93G Mb is a six-coordinate, high-spin complex with a trans water ligand. We have also characterized these derivatives with magnetic circular dichroism (MCD) and electronic absorption (EA) spectroscopy.

MATERIALS AND METHODS

Chemicals and Proteins

All chemicals were of reagent grade or better and were purchased from Sigma-Aldrich. The H93G sperm whale Mb *E. coli* expression system was a gift from Prof. Steven G. Boxer, Stanford University. H93G Mb mutant growth and purification yields pure H93G Mb with imidazole bound in the proximal cavity. For crystallization purposes, we have removed the imidazole using a different method than previously reported (12). First, complete oxidation of the heme iron was accomplished by addition of a few crystals of potassium ferricyanide (Fluka) followed by dialysis (three times) for H93G Mb in 100 mM potassium phosphate buffer at pH 7.0. After eluting a few times (generally 2 or 3) through a BioGel P100 size-exclusion column, the pure ligand-free ferric H93G Mb was collected. This fresh H93G ligand-free Mb sample was buffer exchanged to 100 mM PIPES pH 6.2 buffer in a centricon (8000 nominal molecular weight limit) by centrifuging at 3000 rpm. The final EA spectrum was identical to that previously reported for ligand-free H93G Mb (12).

Crystallization

Crystals of H93G Mb were grown by the vapor diffusion method using the hanging-drop setup at conditions similar to those reported previously (14), but with 100-fold lower imidazole concentration. The protein solution was 0.9 mM (15 mg/mL) 0.05 mM imidazole; the precipitant solution was 37% PEG 8K, 300 mM sodium acetate, 0.1 M PIPES pH 6.2, and

0.1% dioxane. Attempts to grow crystals entirely without imidazole were not successful. Crystals were transferred to two pre-equilibrated drops containing precipitant solution (thus without imidazole) one of which contained 5 mM BME. Crystals were soaked for approximately 10 hours and transferred to cryoprotectant solutions which were the soaking solutions with 10% ethylene glycol. After brief soak, they were flash-cooled in N_2 vapors at -178°C.

Crystallography

Data were collected on two soaked H93G mutant crystals with approximate dimensions of 0.25 × 0.50 × 0.25 mm (BME) and 1.0 × 0.50 × 0.25 mm (no BME). The X-ray diffraction experiments were carried out at the SBC-CAT BM (19BM) beamline of the Advanced Photon Source at Argonne National Laboratory and processed with the HKL 2000 suit of programs (31).

The main parameters for data collection and processing are in Table 1. The crystals were isomorphic with those reported earlier and the initial model for the refinement was obtained from the structure (PDB code 1DTM) of the mutant with a methyl-imidazole ligand (14) by omitting non-protein atoms. Crystallographic refinement was carried out with iterative combination of interactive graphics utilizing Turbo-Frodo software (32) and simulated annealing using CNS software (33). A planar model for the heme was used in agreement with the small molecule data obtained (34) for a similar system (vide infra) with restrains generated using the HIC-Up website (xray.bmc.uu.se/hicup) for the CNS refinements and SHELXPRO for SHELX (35). Water molecules were assigned to peaks that were present in both F_oF_c and $2F_oF_c$ sigmaa weighted maps and formed appropriate contacts with the protein molecule. Water molecules that had a B-factor above 65 $Å^2$ after refinement were deleted. Subsequently, both structures were refined with SHELXL (35) using anisotropic temperature factors. For the BME complex, the free-R increased indicating that the resolution (number of reflections) was insufficient for the anisotropic description of thermal motion and this model was not used further. Correctness of the final structures was evaluated using PROCHECK (36). Figure 1 was obtained with Turbo-Frodo; Figure 2 was generated using Pymol (37). Figure 3 was made with MOLSCRIPT (38) and Raster3D (39). The final refinement parameters are in Table 1.

Spectroscopic Sample Preparation

Mb concentrations were determined by the pyridine hemochromogen method (40). MCD and EA spectral measurements were obtained at 4°C with Mb (~50 μM) in 100 mM potassium phosphate buffer (pH 7.0). For titration experiments, small aliquots of 850 mM potassium acetate or benzoate in 100 mM potassium phosphate buffer or of 2.0 M BME in DMSO were added to 0.4 mL (l = 1 cm, [protein] = ~50 μM) or 2 mL (l = 1 cm, [protein] = ~ 5 μM). Comparable amounts of DMSO did not produce spectral changes. Dissociation constants (K_d) were determined by Hill [see "Data Analysis" in ref. (40)] and double reciprocal plots (41).

Spectroscopic Techniques

EA spectra were recorded with a Cary 400 spectrophotometer or a JASCO J600A spectropolarimeter. MCD spectra were measured in a 0.2 cm cuvette at a magnetic field of 1.41 T with the JASCO J600A spectropolarimeter as described (41). Data acquisition and manipulation were done as reported (42), with JASCO software.

RESULTS

X-ray Crystallography of Ferric H93G·BME and H93G·Acetate Mb

Electron density for both H93G Mb derivatives covered the whole molecule with the exception of a few side chains of surface residues. The electron density for the heme and its proximal and distal ligands is shown in Figure 1. The replacement of His-93 with Gly results in only minor alterations of the Mb structure (6). A comparison of the fold of the imidazole ligated H93G protein (6) with those containing BME or acetate ligands reveals even fewer differences. Taking into account different software packages used in crystallographic refinements, the differences do not appear to be significant except at the N-terminus. The heme iron coordination environments of the BME and acetate complexes of ferric H93G Mb are shown in Figure 2. Differences caused by ligand binding are mostly limited to the immediate environment of the heme.

The superposition of the ferric H93G Mb heme environments of the BME and acetate structures as well as that of the 4-methylimidazole adduct (14) are shown in Figure 3. It is apparent that the three ligands use the same region of the proximal cavity. There are only minor differences in the conformation of the heme propionate chains.

Structure of Ferric H93G·BME Mb and Comparison with Cytochrome P450-CAM

There are many P450 structures in the Protein Data Bank and discussing all of them would be beyond the scope of the present paper. For comparison with the H93G·BME complex, we have selected the structure of the ferric P450-CAM camphor complex, which is the most suitable model by virtue of its five coordinate high-spin Fe^{3+} ion and high precision. The structure was originally reported by Poulos and coworkers (43) and, more recently, by Schlichting et al. (44); we will refer to it (PDB entry 1DZ4) below as P450-CAM. This structure contains two symmetry independent molecules in the unit cell. As in H93G·BME, there are no distal ligands closer to the Fe^{3+} ion than 4 Å. The S-atom of BME is located within experimental error above the Fe^{3+} on the line perpendicular to the porphyrin plane.

The same situation was observed in a small molecule analogue, the *para*-nitrothiophenol thiolate complex of ferric protoporphyrin IX (FePSNP), reported by Tang et al. (34). In P450-CAM, the S_γ atom of the proximal cysteine is somewhat displaced off from the heme center and the S_γ-Fe^{3+} bonds form angles of 83° and 82° (in the two molecules of the unit cell) to the porphyrin plane. In H93G·BME, the Fe^{3+}-S-C angle is 111°, suggesting that the sulfur is sp^3 hybridized and that the Fe-S bond is covalent. A similar situation is seen in P450-CAM where this angle is 108° and 110°. The length of S-Fe^{3+} bond is 2.41Å in H93G·BME, 2.37 Å and 2.36 Å in P450 and 2.324 Å in FePSNP. The distance between the tetrapyrrole plane and Fe^{3+} is 0.5 Å in H93G·BME while 0.4 Å and 0.4 Å in P450, 0.45 Å in FePSNP; these minor differences may reflect different geometrical restraints used for the heme in crystallographic refinements. In conclusion, the geometrical parameters of H93G·BME suggest that this complex is an excellent structural model for high-spin, five-coordinate, ferric cytochrome P450.

Although the proximal cavity can accommodate ligands larger than the BME molecule, we did not observe localized water molecules inside the cavity. The BME hydroxyl forms a 3.3 Å contact with the carbonyl of Leu-89, a distance longer than typical O-H···O hydrogen bonds (45).

The numerous well-documented examples of cysteine ligation in metalloproteins, particularly heme proteins, always involve deprotonated cysteinate. Factors contributing to stabilizing cysteinate binding to Fe so that it is retained in ferrous, ferric and ferryl oxidation states have been discussed (4,10). Hydrogen bonding between the proximal amide (N-H···S) and the

thiolate is a prominent feature. Interestingly, when BME is bound to the heme iron in H93G Mb, it appears to have a weak intramolecular H-bond between its hydroxyl proton and the bound thiolate sulfur that mimics the hydrogen bonds to the proximal cysteinate sulfur seen in P450-CAM (Figure 1A). We also note that the distal side of the BME bound H93G Mb shows an uncoordinated water molecule 4.2 Å away from the heme iron, but within hydrogen bonding distance to the distal His-64 (3.0 Å).

Structure of Ferric H93G·Acetate Mb

In general, the heme module in the acetate adduct of ferric H93G is similar to that observed in ferric Mb (46, PDB entry 1A6K). The Fe^{3+} ion forms a strong bond, 2.26 Å, to the distal water molecule, which also forms a 2.6 Å hydrogen bond to the distal histidine (Table 2). The density for the water molecule is strong, indicating full occupancy, but its shape deviates from spherical (Figure 1B). This suggests some caution in the accuracy assessment of the Fe-O bond length. The distance from the iron to the inner oxygen atom of the acetate ion is 2.22 Å. The ion is not oriented with one of its lone electron pairs towards the Fe^{3+} ion (Figure 4); the Fe^{3+}-O-C angle is 152° and the angle between the acetate plane and the tetrapyrrole plane is 69° indicating that the interaction between the Fe^{3+} and acetate ions is primarily ionic. The outer oxygen atom of the acetate ion is located 2.86 Å from the hydroxyl of Ser-89 indicating the presence of a hydrogen bond.

Spectroscopic Properties of Ferric H93G·BME Mb

Figure 4 shows the EA spectral changes that occur upon addition of BME to ferric, ligand-free H93G Mb. Exogenous, ligand-free, ferric H93G Mb exhibits a Soret absorption peak at 405 nm (12) while the five-coordinate H93G·Mb BME adduct shows a Soret absorption peak at 391 nm and a prominent peak at 618 nm that is typical of high-spin ferric heme complexes. The MCD spectrum of H93G·BME Mb has a unique trough in the Soret region at 390 nm (intensity, -18 $M^{-1}cm^{-1}T^{-1}$) that is typical of a five-coordinate thiolate-ligated ferric heme (9, 17). This spectrum is almost identical to that of camphor-bound ferric P450-CAM as shown in Figure 4. Importantly, the near match is an improvement over the data reported for ferric H93G (ethanethiolate) Mb (10), likely due to the presence of the hydrogen bond to the thiolate sulfur in the ferric H93G BME adduct. The titration data for BME binding to ferric H93G Mb (Supplemental Data, Figure S1) shows that a 1:1 BME complex forms with a K_d value of ~ 7 μM. The ferric H93G·BME Mb complex therefore provides an excellent protein-derived structural model system for the high-spin ferric state of thiolate-ligated P450 proteins.

Spectroscopic Properties of Ferric H93G·Acetate Mb

Titration of exogenous, ligand-free, ferric H93G Mb with acetate (Supplemental Data, Figure S2) reveals the formation of a 1:1 acetate-bound ferric heme derivative with a dissociation constant (K_d) of 440 μM. Similarly, titration with benzoate led to formation of the corresponding 1:1 benzoate adduct with a K_d value of 3.5 mM (data not shown). The X-ray crystal structure (Figures 1B and 2B) of the acetate complex shows that it is a six-coordinate complex with proximal acetate and distal water as axial ligands to the heme iron. The MCD and EA spectra of acetate- and benzoate-ligated ferric H93G Mb are compared in Figure 5. Both MCD spectra have a derivative-shaped feature in the Soret region centered at 410 nm. The derivative-shaped features in the visible region are relatively less intense (~ ± 5 $M^{-1}cm^{-1}T^{-1}$) for both complexes. The EA spectra feature peaks at 626 nm for the benzoate complex and at 614 nm for the acetate adduct that are typical of high-spin ferric heme derivatives. The close similarity between the EA and MCD spectra of the two complexes argues strongly that both have the same heme iron coordination structures.

The Soret absorption peaks of the acetate and benzoate complexes have red-shifted 2 to 3 nm from the value of 405 nm observed for ligand-free H93G Mb (12). Exogenous, ligand-free,

ferric H93G Mb has been established to contain a mixture of five- and six-coordinate water/hydroxide ligation at neutral pH (12). The shift in the Soret absorption peak to ~408 nm could be due to complete homogenous formation of a six-coordinate complex. This is further confirmed by the similar MCD spectra seen for both the acetate and benzoate complexes featuring an intense derivative-shaped feature in the visible region that is distinctly different from what is seen for the five-coordinate carboxylate-bound H25A variant of heme oxygenase (the Soret absorption peak for the latter is at 400 nm) (12). Therefore, based on the crystal structure for acetate-bound H93G and the similarity of the MCD and EA spectral features of the acetate and benzoate adducts, we conclude that both complexes are good structural models for six-coordinate, oxyanion and water-ligated high-spin states of heme proteins.

DISCUSSION

The ability to obtain crystals of H93G at a very low imidazole concentration and subsequent diffusing in ligands into the proximal cavity opens the possibility for further crystal binding studies. It can be speculated that the need for sub-stoichiometric quantities of imidazole during crystallization (1:20 ligand-protein ratio) is related to its role in crystal nucleation or perhaps in protein unfolding/refolding, but it is also possible that the native crystals included the imidazole complex. The soaking solutions did not contain imidazole and if imidazole was present in the native crystals it was replaced by BME (5 mM) during the soaking process. In the absence of BME, acetate (300 mM) from the crystallization media occupies the proximal cavity balancing charges and stabilizing the protein. Reducing the acetate concentration in future crystal soaking experiments may further facilitate proximal ligand exchange.

H93G·BME complex is the first crystal structure that shows how a globin can structurally mimic high-spin, ferric P450 and confirms the predictions derived from MCD data that the H93G complexes with thiolate ligands are five-coordinate (10). MCD characterization of other H93G thiolate adducts with the Fe-S bond indicates that, like the H93G·BME complex, these compounds are five-coordinate with a high-spin ferric iron.

Studies of H93G complexes with imidazoles showed that the proximal side is the preferred location for initial ligand binding in H93G adducts (6,14). Our results extend this finding to two new classes of ligands. The BME molecule has only weak interactions with residues lining the proximal cavity; its position is determined by the Fe-S bond with the rotation around it stabilized by a contact with Leu-89, Figure 2A. It is remarkable that the Fe-S bond in P450-CAM has a very similar geometry despite the constraints resulting from the covalent linkage of the thiolate to the protein frame. Apparently, evolution led to the geometric optimization of the P450 proximal Fe-S(cysteinate) bond.

Why do exogenous ligands prefer to bind on the proximal side of the ferric H93G·Mb cavity mutant? Modeling studies (not shown) indicate that steric hindrance by the distal histidine (His-64) and by Val-68 do not allow positioning of BME and acetate ligands on the distal side without large conformational changes. While movement of the distal histidine of globins out of the pocket has been observed either as a result of very low pH (47) or the binding of aromatic molecules such as imidazole as a heme ligand (48) or iodophenol as an adduct in the distal pocket (49), this clearly is a higher energy conformational state. The enlargement of the proximal cavity in the H93G variant apparently enables ligand binding without transition to this state.

The H93G·Acetate structure (Figure 2B) represents a very unusual environment for heme iron in which a carboxylate oxyanion is the proximal ligand. Previous spectroscopic studies of H93G with oxyanion proximal ligands (11) have provided evidence for a six-coordinate high-spin benzoate/water adduct, in excellent agreement with the results presented herein, and for

a five-coordinate high-spin phenolate complex, i.e., with no distal water. This clearly reflects sensitivity for distal water ligation to the heme iron center that depends on parameters more subtle than just the identity of the proximal ligand donor atom. From the available data for H93G Mb, we propose that the main factor controlling the coordination structure in oxyanion-ligated complexes is the propensity of proximal ligand for charge transfer (push) as assessed by ligand basicity. The acetate ($pK_a = 4.7$) and benzoate ($pK_a = 4.2$) ions are only weakly basic and do not provide enough electron donation to the ferric heme iron. Consequently, an additional water ligand on the distal side is needed. In ferric H93G, in the absence of exogenous ligands, a mixture of five- and six-coordination involving hydroxide and water is seen (12). In contrast, the more basic phenolate ion ($pK_a = 9.9$) yields a five-coordinate structure (11).

In summary, the crystal structures of the ferric H93G Mb cavity mutant with thiolate and carboxylate proximal ligands have been reported at 1.7 and 1.4 Å resolution, respectively. The H93G Mb·BME thiolate adduct is five-coordinate with a covalent 2.41 Å Fe-S bond. The bound BME appears to have an intramolecular hydrogen bond from the alcohol hydroxyl to the ligated thiolate sulfur, mimicking one of the (amide)N-H···S(Cys) hydrogen bonds in cytochrome P450. Thus, the H93G·BME complex provides an excellent protein-based structural model for high-spin ferric P450. In fact, the Fe-S bond in P450-CAM has essentially the same geometry despite the constraints resulting from the covalent linkage of the thiolate to the protein frame. This suggests that evolution led to the geometric optimization of the P450 proximal Fe-S (cysteinate) bond. The H93G Mb acetate complex is six-coordinate with proximal acetate and distal water axial ligands. The Fe-acetate bonding geometry is more consistent with ionic bonding. The structural conclusions drawn from the data presented herein are in excellent agreement with previously reported spectroscopic data and validate the use of cavity mutants as a tool for heme protein investigations. They also provide the first structural evidence that non-imidazole exogenous ligands bind in the proximal ligation site of the H93G myoglobin cavity mutant.

Supplementary Material

Refer to Web version on PubMed Central for supplementary material.

ACKNOWLEDGMENT

References

1. Dawson JH, Pond AE, Roach MP. The H93G myoglobin cavity mutant as a versatile template for modeling heme proteins: MCD studies of thiolate- and imidazole-ligated complexes. Biopolymers (Biospectroscopy) 2002;67:200–206. [PubMed: 12012432]

2. Sono M, Roach MP, Coulter ED, Dawson JH. Heme-containing oxygenases. Chemical Reviews 1996;96:2841–2887. [PubMed: 11848843]

3. Dawson JH. Probing structure function relations in heme-containing oxygenases and peroxidases. Science 1988;240:433–4399. [PubMed: 3358128]

4. Poulos TL. The role of the proximal ligand in heme enzymes. J. Biol. Inorg. Chem 1996;1:356–359.

5. Rydberg P, Sigfridsson E, Ryde U. On the role of the axial ligand in heme proteins: a theoretical study. J. Biol. Inorg. Chem 2004;9:203–223. [PubMed: 14727167]

6. Barrick D. Replacement of the proximal ligand of sperm whale myoglobin with free imidazole in the mutant His93Gly. Biochemistry 1994;33:6546–6554. [PubMed: 8204590]

7. Pond AE, Roach MP, Thomas MR, Boxer SG, Dawson JH. The H93G myoglobin cavity mutant as a versatile template for modeling heme proteins: Ferrous, ferric and ferryl mixed ligand complexes with imidazole in the cavity. Inorg. Chem 2000;39:6061–6066. [PubMed: 11151505]

8. Das TK, Franzen S, Pond AE, Dawson JH, Rousseau DL. Formation of a five-coordinate hydroxide-bound heme in the His93Gly mutant of sperm whale myoglobin. Inorg. Chem 1999;38:1952–1953. [PubMed: 11670970]

9. Franzen S, Peterson ES, Brown D, Friedman JM, Thomas MR, Boxer SG. Proximal ligand motions in H93G myoglobin. Eur. J. Biochem 2002;269:4879–4886. [PubMed: 12354119]

10. Roach MP, Pond AE, Thomas MR, Boxer SG, Dawson JH. The role of the distal and proximal protein environments in controlling the ferric spin state and in stabilizing thiolate ligation in heme systems: Thiolate adducts of the myoglobin H93G cavity mutant. J. Am. Chem. Soc 1999;121:12088–12093.

11. Roach MP, Puspita WJ, Watanabe Y. Proximal ligand control of heme iron coordination structure and reactivity with hydrogen peroxide: investigations of the myoglobin cavity mutant H93G with unnatural oxygen donor proximal ligands. J. Inorg. Biochem 2000;81:173–182. [PubMed: 11051562]

12. Pond AE, Roach MP, Sono M, Rux AH, Franzen S, Hu R, Thomas MR, Wilks A, Dou K, Ikeda-Saito M, Ortiz de Montellano PR, Woodruff WH, Boxer SG, Dawson JH. Assignment of the heme axial ligand(s) for the ferric myoglobin (H93G) and heme oxygenase (H25A) cavity mutants as oxygen donors using magnetic circular dichroism. Biochemistry 1999;38:7601–7608. [PubMed: 10360958]

13. Perera R, Dawson JH. Modeling heme protein active sites with the His93Gly cavity mutant of sperm whale myoglobin: Complexes with nitrogen-, oxygen- and sulfur-donor proximal ligands. J. Porphyrins Phthalocyanines 2004;8:246–254.

14. Barrick D, Dahlquist FW. Trans-substitution of the proximal hydrogen bond in myoglobin: I. Structural consequences of hydrogen bond deletion. Protein Sci 2000;39:278–290.

15. Franzen S, Bailey J, Dyer RB, Woodruff WH, Hu RB, Thomas MR, Boxer SG. A photolysis-triggered heme ligand switch in H93G myoglobin. Biochemistry 2001;40:5299–5305. [PubMed: 11318654]

16. Cao W, Ye X, Sjodin T, Christian JF, Demidov AA, Berezhna S, Wang W, Barrick D, Sage T, Champion PM. Investigations of photolysis and rebinding kinetics in myoglobin using proximal ligand replacements. Biochemistry 2004;43:11109–11117. [PubMed: 15323570]

17. Dawson JH, Holm RH, Trudell JR, Barth G, Linder RE, Bunnenberg E, Djerassi C, Tang SC. Oxidized cytochrome P-450. Magnetic circular dichroism evidence for thiolate ligation in the substrate-bound form. Implications for the catalytic mechanism. J. Am. Chem. Soc 1976;98:3707–3709. [PubMed: 1270706]

18. Yoshioka S, Takahashi S, Ishimori K, Morishima I. Roles of the axial push effect in Cyt P450cam studied with the site-directed mutagenesis at the heme proximal site. J. Inorg. Biochem 2000;81:141–151. [PubMed: 11051559]

19. Ueyama N, Nishikawa N, Yamada Y, Okamura T, Nakamura A. Cytochrome P450 model (porphinato)(thiolato)iron(III) complexes with single and double NH···S hydrogen bonds at the thiolate site. J. Am. Chem. Soc 1996;118:12826–12827.

20. Matsui T, Shingo N, Ishimori K, Watanabe Y, Morishima I. Preparation and reactions of myoglobin mutants bearing both proximal cysteine ligand and hydrophobic distal cavity: Protein models for the active site of P450. Biochemistry 1996;35:13118–13124. [PubMed: 8855949]

21. Hildebrand DP, Ferrer JC, Tang HL, Smith M, Mauk AG. Trans effects on cysteine ligation in the proximal His93Cys variant of horse heart myoglobin. Biochemistry 1995;34:11598–11605. [PubMed: 7547891]

22. Nagai M, Yoneyama Y, Kitagawa T. Characteristics in tyrosine coordinations of four hemoglobins M probed by resonance Raman spectroscopy. Biochemistry 1989;28:2418–2422. [PubMed: 2730874]

23. Nagai M, Yoneyama Y. Reduction of methemoglobins M Hyde Park, M Saskatoon, and M Milwaukee by ferredoxin and ferredoxin-nicotinamide adenine dinucleotide phosphate reductase system. J. Biol. Chem 1983;258:14379–14384. [PubMed: 6643489]

24. Perutz MF, Pulsinelli PD, Ranney HM. Structure and subunit interaction of haemoglobin M Milwaukee. Nat. New Biol 1972;237:259–263. [PubMed: 4338724]

25. Greer J. Three-dimensional structure of abnormal human haemoglobins M Hyde Park and M Iwate. J. Mol. Biol 1971;59:107–126. [PubMed: 5283749]

26. Pulsinelli PD, Perutz MF, Nagel RL. Structure of hemoglobin M Boston, a variant with a five-coordinated ferric heme. Proc Natl Acad Sci U S A 1973;70:3870–3874. [PubMed: 4521212]

27. Abraham BD, Sono M, Boutard O, Shriner A, Dawson JH, Brash AR, Gaffney BJ. Characterization of the coral allene oxide synthase active site with MCD and EPR spectroscopy. Evidence for tyrosinate ligation to the enzyme heme iron. Biochemistry 2001;40:2251–2259. [PubMed: 11329294]

28. Adachi S, Nagano S, Ishimori K, Watanabe Y, Morishima I, Egawa T, Kitagawa T, Makino R. Roles of proximal ligand in heme proteins: Replacement of proximal histidine of human myoglobin with cysteine and tyrosine by site-directed mutagenesis as models for P-450, chloroperoxidase, and catalase. Biochemistry 1993;32:241–252. [PubMed: 8380334]

29. Hildebrand DP, Burk DL, Maurus R, Ferrer JC, Brayer GD, Mauk AG. The proximal ligand variant His93Tyr of horse heart myoglobin. Biochemistry 1995;34:1997–2005. [PubMed: 7849057]

30. Perera, R. Ph.D. Thesis. University of South Carolina; 2005. Chapter 7

31. Otwinowski Z, Minor W. Processing of X-ray diffraction data collected in oscillation mode. Methods Enzym 1997;276:307–326.

32. Russel, A.; Cambillau, C. Mountain View Ca. Silicon Graphics. 1991. "Turbo Frodo" Silicon Graphics Geometry Partners Directory; p. 86

33. Brunger AT, Adams PD, Clore GM, Delano WL, Gros P, Grosse-Kunstleve, Reed RJ, Jiang J, Kuszewskic J, Nilges M, Pannu N, Read RJ, Rice LM, Simonson T, Warren GL. Crystallography and NMR System: A new software suite for macromolecular structure determination. Acta Crystallogr 1998;D54:905–921.

34. Tang SC, Koch S, Papaefthymiou GC, Foner S, Frankel RB, Ibers JA, Holm RH. Axial ligation modes in iron(III) porphyrins. Models for the oxidized reaction states of cytochrome P450 enzymes and the molecular structure of iron(III) protoporphyrin IX dimethyl ester p-nitrobenzenethiolate. J. Am. Chem. Soc 1976;98:2414–2434. [PubMed: 177476]

35. Sheldrick, G. 1997. http://shelx.uni-ac.gwdg.de/SHELX/

36. Laskowski RA, MacArthur MW, Moss DS, Thornton JM. PROCHECK: a program to check the stereochemical quality of protein structures. J. Appl. Crystallog 1993;26:283–291.

37. Delano Scientific LLC. http://www.pymol.org

38. Kraulis PJ. MOLSCRIPT: a program to produce both detailed and schematic plots of protein structures. J. Appl. Crystallog 1991;24:946–950.

39. Merritt EA, Bacon DJ. Raster3D: photorealistic molecular graphics. Methods Enzymol 1997;277:505–524. [PubMed: 18488322]

40. Sono M, Andersson LA, Dawson JH. Spectroscopic investigations of ferric cytochrome P450-CAM ligand complexes. Identification of the ligand trans to cysteinate in the native enzyme. J. Biol. Chem 1982;257:3606–3617. [PubMed: 6277939]

41. Sono M, Andersson LA, Dawson JH. Sulfur donor ligand binding to ferric cytochrome P450-CAM and myoglobin. Ultraviolet-visible absorption, magnetic circular dichroism, and electron paramagnetic resonance spectroscopic investigation of the complexes. J. Biol. Chem 1982;257:8308–8320. [PubMed: 6282878]

42. Huff AM, Chang CK, Cooper DK, Smith KM, Dawson JH. Imidazole- and alkylamine-ligated iron (II, III) chlorin complexes as models for histidine and lysine coordination to the iron in dihydroporphyrin-containing proteins: Characterization with magnetic circular dichroism spectroscopy. Inorg. Chem 1993;32:1460–1466.

43. Poulos TL, Finzel BC, Howard AJ. High resolution crystal structure of cytochrome P450cam. J. Mol. Biol 1987;195:687–700. [PubMed: 3656428]

44. Schlichting I, Berendzen J, Chu K, Stock AM, Maves SA, Benson DE, Sweet RM, Ringe D, Petsko GA, Sligar SG. The catalytic pathway of cytochrome P450cam at atomic resolution. Science 2000;287:1615–1622. [PubMed: 10698731]

45. Jeffrey, GA.; Saenger, W. Hydrogen Bonding in Biological Structures. Springer-Verlag; Berlin: 1991. p. 29-31.

46. Vojtechovsky J, Chu K, Berendzen J, Sweet RM, Schlichting I. Crystal structures of myoglobin-ligand complexes at near-atomic resolution. Biophys. J 1999;77:2153–2174. [PubMed: 10512835]

47. Yang F, Phillips GN. Crystal structures of CO-, deoxy- and met-myoglobin at various pH values. J. Mol. Biol 1996;256:762–774. [PubMed: 8642596]

48. Lionetti C, Guanziroli MG, Frigerio F, Ascenzi P, Bolognesi M. X-ray crystal structure of the ferric sperm whale myoglobin: Imidazole complex at 2.0 Å resolution. J. Mol. Biol 1991;217:409–412. [PubMed: 1994031]

49. LaCount MW, Zhang E, Chen YP, Han K, Whitton MM, Lincoln DE, Woodin SA, Lebioda L. The crystal structure and amino acid sequence of dehaloperoxidase from *Amphitrite ornata* indicate common ancestry with globins. J. Biol. Chem 2000;275:18712–18716. [PubMed: 10751397]
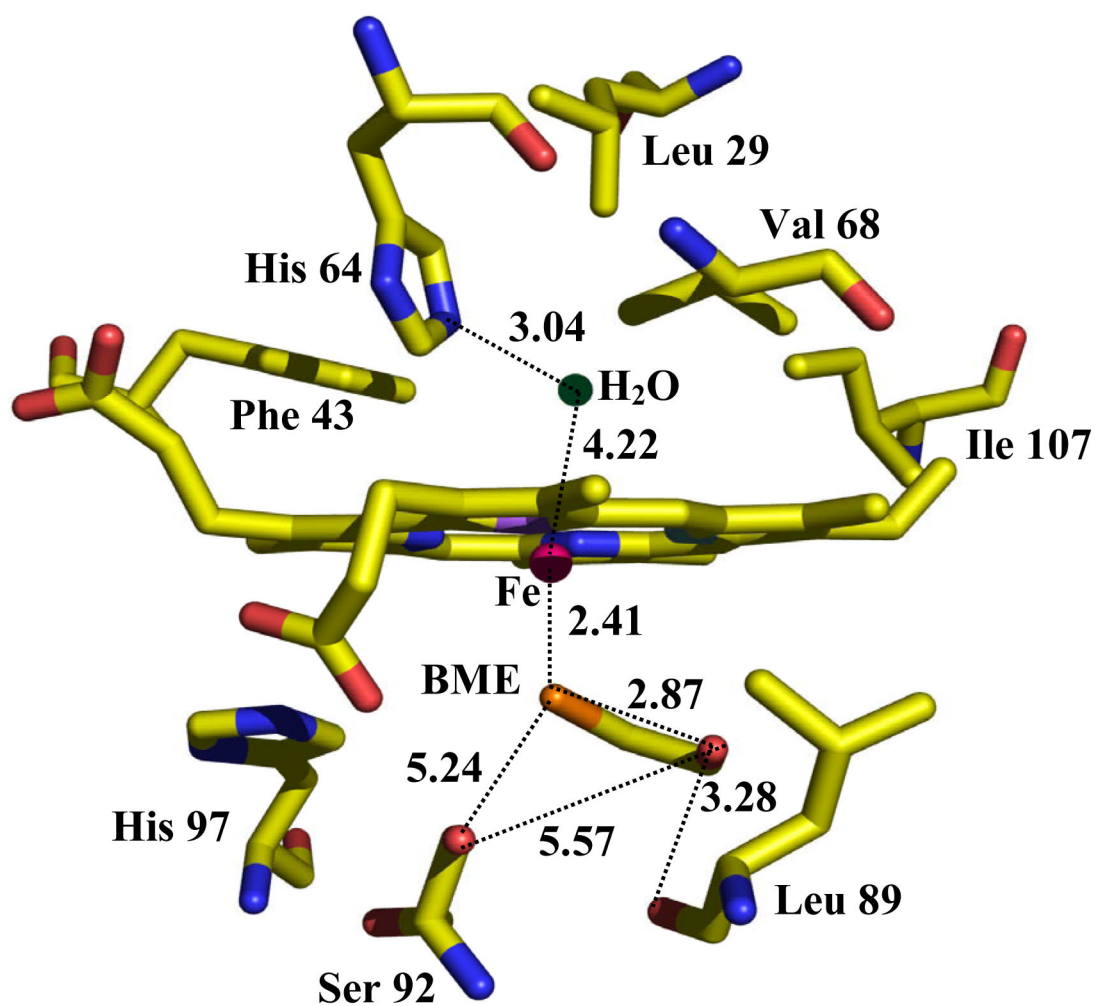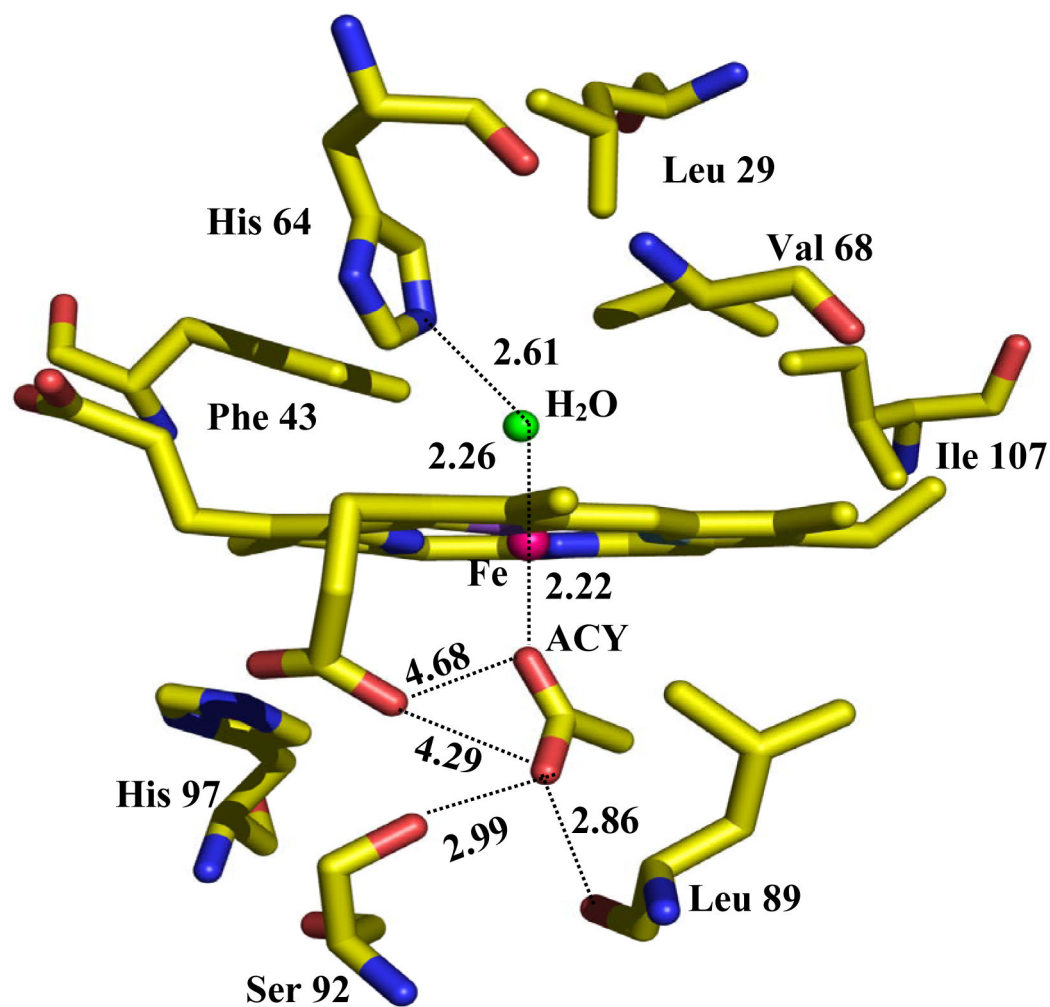
A
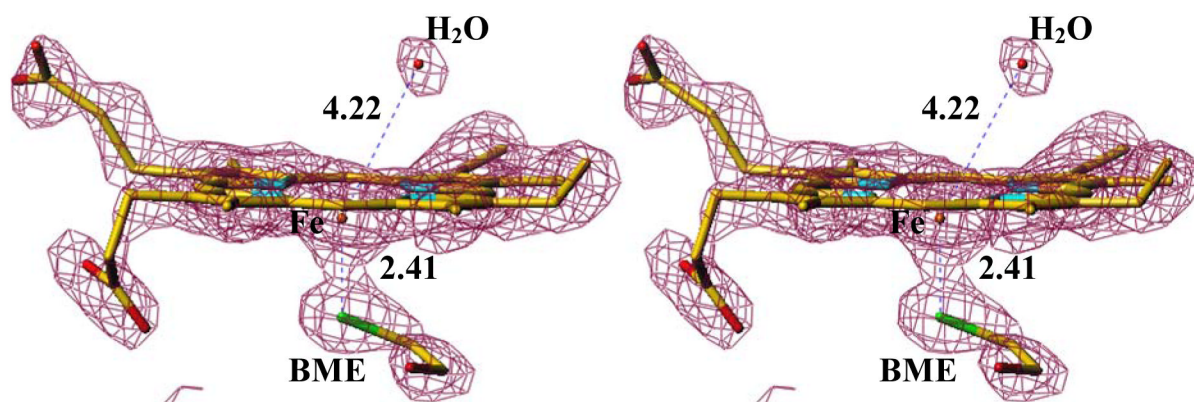
B
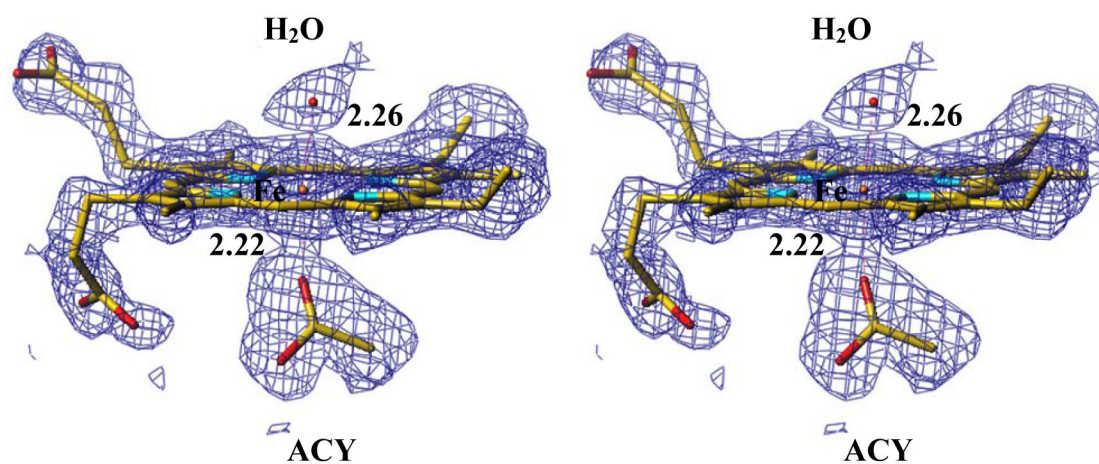
Figure 1.
Stereo diagram of the omit electron density calculated as an F_oF_c map, contoured at 5σ level: (A) for the heme and the BME molecule, (B) for the heme and for the acetate ion.
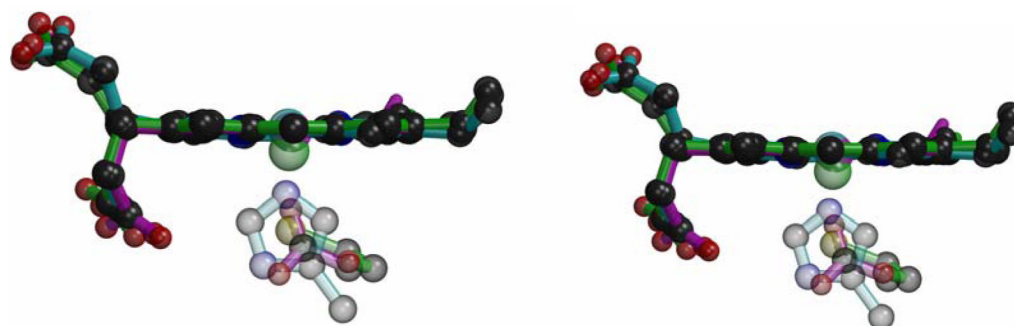
A

B

Figure 2.
Schematic representation of the heme iron environment in ferric H93G Mb (A) with β-mercaptoethanol bound in the proximal cavity and (B) with acetate bound in the proximal cavity and a water molecule coordinated in the distal pocket, as determined by X-ray crystallography.

Figure 3.
Stereo view of superposition of the hemes in BME, acetate and 4-methyl-imidazole
(determined by Barrick (27)) complexes based on protein C_α. positions. Bonds are colored:
heme and BME in BME complex, green; heme and acetate in acetate complex, magenta; heme
and 4-methyl-imidazole in 4-methyl-imidazole complex, blue. Fe atoms are colored in the same
way as its bond color. Other atoms are colored: C, black; O, red; N, blue; S, yellow.
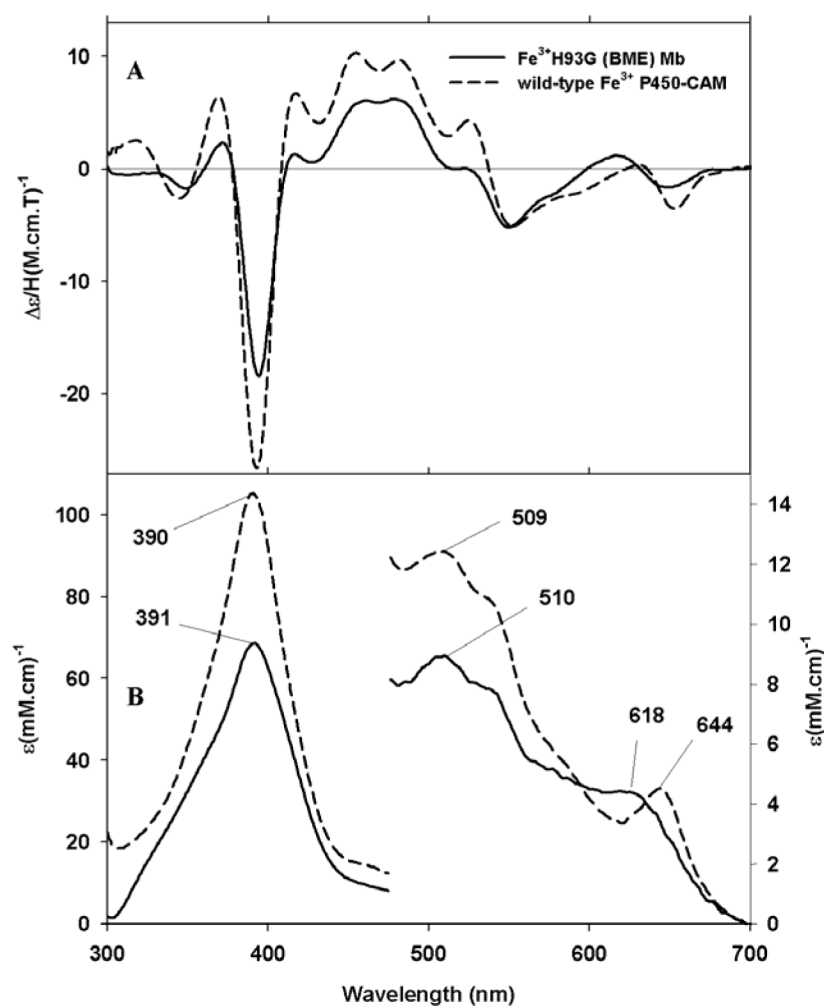
Figure 4.
Magnetic circular dichroism (A) and electronic absorption (B) spectra of five coordinate, high-spin ferric BME-bound H93G Mb (1.14 mM BME and ~50 μM H93G) (solid line) and wild type P450-CAM in the presence of camphor (1 mM) (dashed line). See Materials and Methods for additional details.
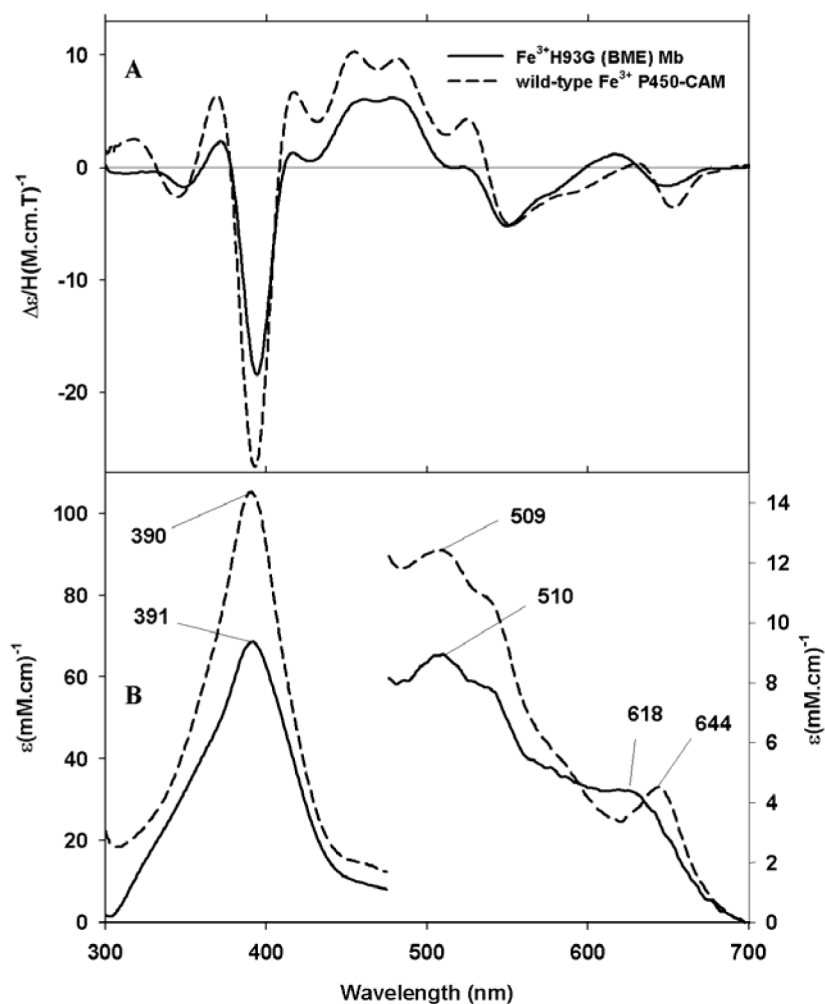
Figure 5.
Magnetic circular dichroism (A) and electronic absorption (B) spectra of six coordinate, high-spin ferric H93G Mb (~50 μM) in the presence of benzoate (16 mM) (dashed line) and acetate (200 mM) (solid line). See Materials and Methods for additional details.

Table 1

Crystallographic Data and Refinement Statistics for H93G complexes with β-mercaptoethanol (BME) and acetate ion

Ligand		BME β-mercaptoethanol	acetate ion
x-ray source		APS SBC-CAT BM	APS SBC-CAT BM
Detector		3 × 3 mosaic	3 × 3 mosaic
Wavelength (Å)		0.97929	0.97929
Temperature		100K	100K
# frames		120	195
Oscillation range (degree)		1.000	1.000
Detector to crystal distance (mm)		130	125
Space group		P2$_1$2$_1$2$_1$	P2$_1$2$_1$2$_1$
Unit cell dimensions:	a (Å)	39.67	39.72
	b (Å)	47.77	48.00
	c (Å)	77.43	77.61
Mosaicity, from HKL2000 (degree)		0.7	0.7
Resolution range (Å) (outer shell)^a		50.0-1.70 (1.76-1.70)	50.0-1.40 (1.45-1.40)
Average I		3823	3804
Average I/σ(I)		10.4	8.9
Number of unique reflections		16,116 (1,269)	26,514 (1,107)
Redundancy		3.4 (2.4)	5.7 (2.2)
Completeness (%)		89.5 (60.5)	88.3 (37.3)
Low resolution linear R-factor in shell		(50.0-3.7) 0.025	(50.0-3.0) 0.026
Total linear and square R-merge^b		0.046 (0.328) 0.039 (0.267)	0.046 (0.608) 0.034 (0.532)
Number of reflections in refinement (with |F|/σ|F|>2)		13,266	20,757
R-value^c		19.4	{11.6}
R$_{free}$ (percent of reflections used)		21.4 (3.7%)	{20.6} (3.3%)
msd, bond lengths (Å)		0.006	0.006
msd, bond angles (deg.)		1.0	1.0
average B factor (Å^2) for protein atoms		21.9	17.4
average B factor (Å^2) for solvent		39.4	34.9
average B factor (Å^2) for the ligand		30.4	18.9
Ramachandran statistics:^{e}			
Residues most favored phi/psi (%)		92.6	91.9
Resid. in additionally allowed region (%)		7.4	8.1
number of water molecules		271	313

^{a}Values in parentheses are for the outermost resolution shell, values in brackets are for the SHELX refinements

^{b}$R_{merge} = (\Sigma_h|I_h - <I>|)/(\Sigma_h I_h)$.

^{c}$R = (\Sigma_h|F_{obs} - F_{cal}|)/(\Sigma_h F_{obs})$.

^{d}R_{free} = crystallographic R-factor for test set30.

^{e}As determined by PROCHECK33.

Table 2

Stereochemistry of the Heme-Axial Ligand Interaction in H93G and Wild-Type Myoglobin

Ligand	H93G BME[a]	H93G Acetate[a]	H93G Imidazole[b]	Wild Type Imidazole[c]
Distance (Å)				
S_b to Fe^{3+} [d]	2.4			
O_a to Fe^{3+} [d]		2.2		
N_t to Fe^{3+} [d]			1.9	2.2
S_b to heme plane	3.0			
O_a to heme plane		2.4		
N to heme plane			1.9	2.4
Fe^{3+} to heme plane	0.5	0.2	0.0	0.2
Fe^{3+} to distal water	4.2	2.3	2.7	2.1
Distal water to His-64 $N_\varepsilon 2$	3.0	2.6	2.7	2.6

[a] From this study.

[b] From the sperm whale myoglobin mutant H93G structure of Barrick (1994).

[c] From the ferric sperm whale myoglobin structure of Takano (1977).

[d] S_b is defined as the sulfur from BME that is bonded to the heme iron; O_a is defined as the oxygen from acetate that is bonded to the heme iron; N_t is defined as the nitrogen from imidazole that is bonded to the heme iron.